

Carrier filtering effect for enhanced thermopower in a body-centered tetragonal ruthenate

Ryota Otsuki,* Yoshiki J. Sato,† Ryuji Okazaki,‡ Tomoya Komine, Ryosuke Kurihara, and Hiroshi Yaguchi
Department of Physics and Astronomy, Tokyo University of Science, Noda 278-8510, Japan

Charged carriers in solids diffuse from hot to cold sides under temperature gradient to induce the thermoelectric voltage. Carrier filtering effect, which only passes either electrons or holes for the conduction process, is an efficient method to enhance such voltage, although it is challenging to experimentally realize it especially in conventional metals with weak energy dependence of the density of states near the Fermi level. Here we measure the in-plane and out-of-plane thermopower of the layered perovskite Sr_2RuO_4 single crystals above room temperature. We find that the out-of-plane thermopower is largely enhanced with increasing temperature, while the in-plane one seems to remain a temperature-independent constant value expected from the Heikes formula. The observed large out-of-plane thermopower may originate from the recently proposed intriguing hole filtering effect in the body-centered tetragonal system, in which the carrier hopping through the centered atom is essential. Thus, the present carrier filtering effect may be a universal property to be applicable in various materials belonging to such crystal system.

I. INTRODUCTION

Thermoelectricity is a solid-state property to convert the heat current into charge one, or vice versa, attracting great attention as an environmentally-friendly energy conversion technology [1–3]. In the fundamental point of view, the thermopower S , which is the proportional coefficient between the electric field \mathbf{E} and the temperature gradient ∇T as $\mathbf{E} = S \nabla T$, serves an intriguing measure of how large the electron-hole asymmetry is in materials [4]; under the temperature gradient, the carrier diffusion from high- to low-temperature sides induces the thermoelectric voltage, the magnitude of which is however significantly cancelled owing to the opposite polarities of the thermally excited electrons and holes. To enhance the thermopower, it is thus important to introduce a sort of asymmetry for the charged carriers: for example, an energy barrier picture to pass only the unipolar carriers has been suggested in the superlattice structures based on the thermionic emission process [5, 6]. In the reciprocal space, a peculiar pudding-mold band shape to explain large thermopower in the cobalt oxides [7–9] is a kind of carrier filtering because it utilizes the large asymmetry in the carrier velocities to increase the thermopower and the electrical conductivity simultaneously. Low-dimensional materials with highly asymmetric energy dependence of the density of states (DOS) are also promising to enhance the thermoelectric efficiency [10] and has been experimentally demonstrated [11–13]. In a real-space picture, a spin blockade hopping in several cobalt oxides also clarifies the asymmetry in the thermoelectric transport [14–20]. Moreover, the electron-hole asymmetry in the scattering rate is also crucial for the thermopower [21, 22].

For such carrier filtering effects, Mravlje and Georges have recently suggested unique filtering mechanism based on the band structure in the body-centered tetragonal (bct) crystal system [Fig. 1(a)] such as the layered ruthenate [23]. In a simple tight-binding picture, the energy dispersion of the bct lattice in such layered materials is given as $\varepsilon(\mathbf{k}) = \varepsilon_1(\mathbf{k}) + \varepsilon_2(\mathbf{k})$,

where $\varepsilon_1(\mathbf{k}) = t_1(\cos k_x + \cos k_y)$ ($t_1 < 0$) is the large in-plane hopping term and $\varepsilon_2(\mathbf{k}) = t_2 \cos(k_x/2) \cos(k_y/2) \cos(k_z/2)$ ($t_2 < 0$, $|t_2| < |t_1|$) represents the out-of-plane hopping one [Fig. 1(b)]. In this case, owing to the in-plane transfer integral t_1 , the energy along the Γ -Z line ($0, 0, k_z$) and the X-X' line ($\pm\pi, \pm\pi, k_z$) yield large negative and positive values, respectively. The out-of-plane velocity along the Γ -Z line then becomes finite because of the dispersion $\varepsilon(0, 0, k_z) = 2t_1 + t_2 \cos(k_z/2)$, while it becomes zero along the X-X' line since $\varepsilon(\pm\pi, \pm\pi, k_z) = -2t_1$. Therefore, the difference in the out-of-plane velocity along the Γ -Z and the X-X' lines becomes significant. This leads to the prominent electron-hole asymmetry when the chemical potential μ locates near the

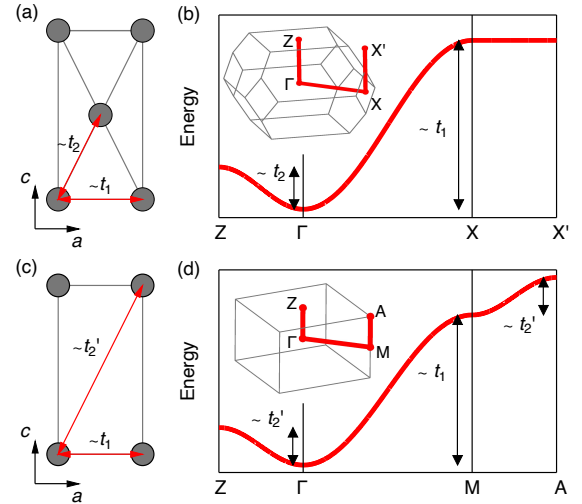


FIG. 1. Concept of the carrier filtering in body-centered tetragonal lattice. (a) Body-centered tetragonal lattice. (b) Tight-binding band dispersion for (a). The inset depicts the Brillouin zone and the notations in Ref. 39 are used. The out-of-plane velocity appears along the Γ -Z line while it vanishes along the X-X' line. The point X' denotes the X point in the adjacent Brillouin zone. (c) Primitive tetragonal lattice. (d) Tight-binding band dispersion for (c). The out-of-plane velocity emerges in both the Γ -Z and the X-X' lines.

* 6223510@ed.tus.ac.jp

† yoshiki_sato@rs.tus.ac.jp

‡ okazaki@rs.tus.ac.jp

middle of the band, and the carrier filtering mechanism operates at high temperatures $T \sim |t_1|/k_B$, where the thermal energy $k_B T$ is a substantial fraction of the bandwidth $|t_1|$. Subsequently large thermopower is expected at such high-temperature range. Note that the situation is distinct from that of the primitive tetragonal structure with the out-of-plane hopping term of $\varepsilon_2(\mathbf{k}) = t'_2 \cos(k_x) \cos(k_y) \cos(k_z)$ [Figs. 1(c) and 1(d)].

The aim of this paper is to experimentally examine such carrier filtering effect in the proposed material Sr_2RuO_4 . The layered perovskite oxide Sr_2RuO_4 with the bct lattice (space group $I4/mmm$) has been extensively studied as a model material to examine the unconventional superconductivity in two dimensions [24–29], while the pairing mechanism of the superconducting state is still a remaining issue [30–35]. Since the electronic structure and the quasi-two-dimensional (q-2D) Fermi surfaces of this material have been well studied both theoretically [36–40] and experimentally [41–45], this material is indeed a minimal model for the examination of such filtering effect, whereas the thermopower measurements on the single-crystalline samples of Sr_2RuO_4 have been limited in the low-temperature range [46–48].

In the present study, we measure the in-plane and out-of-plane thermopower of Sr_2RuO_4 single crystals at high temperatures. The in-plane thermopower is well described within the Heikes formula that has been widely used to explain the high-temperature thermopower of correlated oxides. On the other hand, the out-of-plane thermopower increases with increasing temperature and exceeds the expected value of Heikes formula. These results indicate that the suggested carrier filtering effect is realized in the present bct system. Although the out-of-plane resistivity is relatively large in Sr_2RuO_4 [49], this filtering is very universal for the bct lattice and acts at high temperatures, offering a unique class of efficient thermoelectric materials.

II. METHODS

Single crystals of Sr_2RuO_4 were grown by a floating-zone method [50]. We used the cleaved single crystals for the in-plane thermopower measurements, the photograph of which is shown in Fig. 2(a). For the out-of-plane experiments, the crystal was cut using an electrical discharge machine to obtain the elongated crystal to the c -axis direction [Fig. 2(b)] [51]. The thermopower was measured by a steady-state technique using two platinum resistance thermometers in a tube furnace [52–54]. The thermoelectric voltage of the crystal was measured with a Keithley 2182A nanovoltmeter. The temperature gradient of about 0.5 K/mm was applied using a resistive heater. The thermoelectric voltage from the wire leads (platinum wires) was subtracted.

In order to verify how similar the band structure of Sr_2RuO_4 is to the band dispersion of the simple tight-binding model shown in Fig. 1(b), we also performed first-principles calculations based on density functional theory (DFT) using Quantum Espresso [55–57]. We used the projector-augmented-wave pseudopotentials with the Perdew-Burke-

Ernzerhof generalized-gradient-approximation (PBE-GGA) exchange-correlation functional. The cut-off energies for plane waves and charge densities were set to 70 and 560 Ry, respectively, and the k -point mesh was set to $20 \times 20 \times 20$ uniform grid to ensure the convergence. We used on-site Coulomb energy $U = 3.5$ eV and exchange parameter $J = 0.6$ eV for Ru ions [58] and performed full relativistic calculations with spin-orbit coupling (DFT+ U +SOC). The present calculations are not spin-polarized.

To examine the filtering effect, we also calculated the thermopower based on the linearized Boltzmann equations under constant relaxation time approximation using a Boltzmann module [59]. From the obtained eigenvalues of the n -th band at \mathbf{k} point $E_{n,\mathbf{k}}$, the transport function tensor $L_{ii}(\varepsilon)$ is calculated as

$$L_{ii}(\varepsilon) = \sum_{n,\mathbf{k}} v_i^2 \tau \delta(\varepsilon - E_{n,\mathbf{k}}), \quad (1)$$

where v_i is the i -th component of the group velocity $\mathbf{v} = \frac{1}{\hbar} \nabla_{\mathbf{k}} E_{n,\mathbf{k}}$, τ ($= 10^{-14}$ s) is the relaxation time, and δ is the delta function [59, 60]. Here we consider the diagonal components $ii = xx$ and zz . We then calculated the electrical conductivity tensor $\sigma_{ii}(\mu) = e^2 \int_{-\infty}^{\infty} d\varepsilon \left(-\frac{\partial f_0}{\partial \varepsilon} \right) L_{ii}$, where e is the elementary charge and f_0 is the Fermi-Dirac distribution function for the chemical potential μ and temperature T . Similarly, the Peltier conductivity tensor is calculated as $P_{ii}(\mu) = -\frac{e}{T} \int_{-\infty}^{\infty} d\varepsilon \left(-\frac{\partial f_0}{\partial \varepsilon} \right) (\varepsilon - \mu) L_{ii}$, and the thermopower S_{ii} is obtained as $S_{ii} = P_{ii}/\sigma_{ii}$.

III. RESULTS AND DISCUSSION

A. In-plane thermopower

Figure 2(c) shows the temperature dependence of the in-plane (blue) and out-of-plane (red) thermopower. We first discuss the in-plane thermopower behavior. The room-temperature value of $S \sim 25$ $\mu\text{V}/\text{K}$ well agrees with the earlier reports [46–48], in which the sample dependence was also observed in the magnitude of the thermopower. Above room temperature, the in-plane thermopower exhibits weak temperature dependence, which is similar to the thermopower measured in the polycrystalline samples [61]. This in-plane data may be described by the Heikes formula for the mixed three valence states (atomic states with $N - 1$, N , and $N + 1$ electrons) [23] with the quenched orbital degeneracy due to the dominant Hund's coupling [62, 63]:

$$S = \frac{k_B}{2e} \ln \frac{g_{N-1}}{g_{N+1}}, \quad (2)$$

where k_B is the Boltzmann constant and g_i is the spin degeneracy of the atomic state with i electrons. For Sr_2RuO_4 ($N = 4$), the Heikes thermopower is estimated as $S = k_B/(2e) \ln(g_3/g_5) = k_B/(2e) \ln 2 \approx 30$ $\mu\text{V}/\text{K}$, which is reasonably close to the experimental values. Note that such concentration-independent formula may also be applicable to the high-temperature thermopower in the Mn oxides [64].

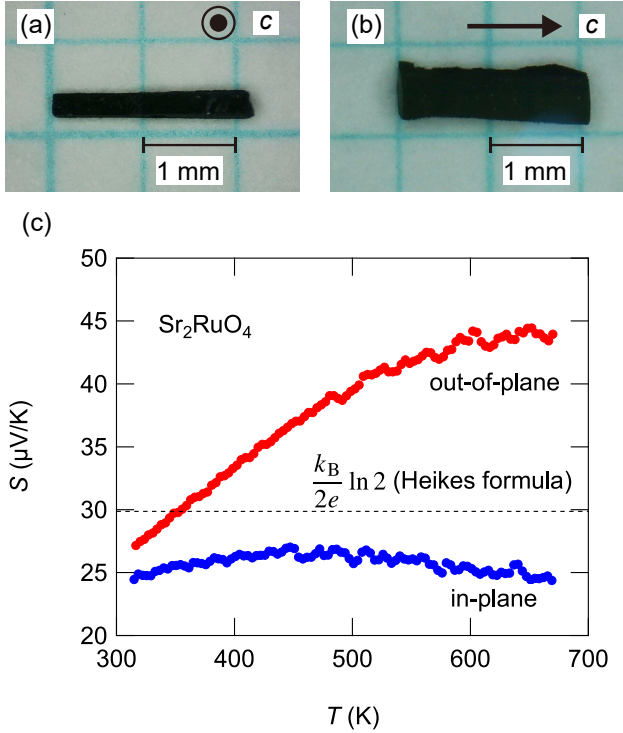


FIG. 2. (a,b) Photograph of the single-crystalline Sr_2RuO_4 samples for the (a) in-plane and (b) out-of-plane thermopower measurements. (c) Temperature dependence of the thermopower S measured for the in-plane (blue) and out-of-plane (red) directions. The dashed line indicates a value expected from the Heikes formula at high temperatures [23].

Figure 3 summarizes the room-temperature thermopower data in various ruthenium oxides as a function of the formal valence of Ru ions. Note that we here focus on the in-plane data and the large out-of-plane thermopower at high temperatures will be discussed in the following section. The thermopower in these ruthenium oxides is almost temperature-independent near room temperature [65, 66], similar to that of the present Sr_2RuO_4 for the in-plane direction. In Fig. 3, the data seems to gather at the valence state of Ru^{4+} with the thermopower value of $S = 30 \mu\text{V/K}$ as mentioned before. In addition, a trend of negative correlation between the thermopower value and the valence is obtained. However, it is difficult to express the overall behavior by the Heikes formula: Eq. (2) is obtained by considering the mixed three valence states and is valid only for $N = 4$, whereas the extended Heikes formula for mixed two valence states shows divergent behavior of the thermopower close to the integer valence state [67–69]. For instance, in the valence range above 4 (mean number of electrons $n < 4$), the Heikes formula becomes

$$S = -\frac{k_B}{e} \ln\left(\frac{g_4}{g_3} \frac{4-n}{n-3}\right), \quad (3)$$

which diverges for the integer values of n . Note that a mixed state with Ru^{4+} ($N = 4$) and Ru^{5+} ($N = 3$) ions is considered

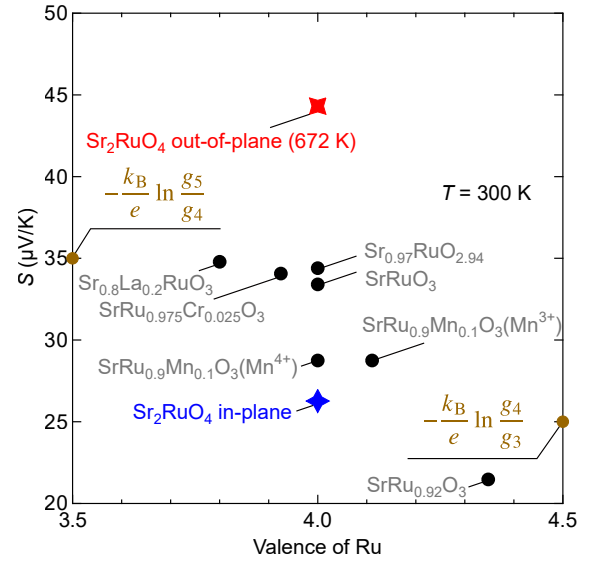


FIG. 3. Thermopower in various itinerant ruthenium oxides as a function of the formal valence of Ru ions. The data were measured at room temperature except for the out-of-plane data of Sr_2RuO_4 . Data in the earlier reports are taken from Ref. 65.

in Eq. (3), in contrast to the situation for Eq. (2) where three valence states are adopted. In Fig. 3, we instead note the expected thermopower of $(-k_B/e) \ln(g_4/g_3) \approx 25 \mu\text{V/K}$ for the formal valence of $\text{Ru}^{4.5+}$ ($n = 3.5$) and $(-k_B/e) \ln(g_5/g_4) \approx 35 \mu\text{V/K}$ for $\text{Ru}^{3.5+}$ ($n = 4.5$). The data seems to locate between these values and it is a future study to elucidate the exact formula to describe the thermopower in the whole valence range.

B. Out-of-plane thermopower

Then we focus on the out-of-plane thermopower, which increases with increasing temperature (Fig. 2) and well exceeds the above mentioned Heikes value of $30 \mu\text{V/K}$ (Fig. 3). This behavior is highly distinct from the conventional trend: as seen in the Heikes formula, the high-temperature thermopower will be expressed as the thermodynamic quantity with no directional anisotropy. Indeed, for the layered cobalt oxides, the in-plane anisotropy in the thermopower gradually diminishes at higher temperatures [53]. Thus, it is clear that the Heikes picture is not applicable to the out-of-plane thermopower at high temperature range in Sr_2RuO_4 . Rather, such a temperature dependence is well consistent with the theoretical estimation to consider the unique carrier filtering effect based on the bct lattice system [23].

To examine such filtering effect for the out-of-plane thermopower, we calculate the band structure along the peculiar k_z line in the DFT(GGA) + U + SOC scheme, since (i) the bandwidth may be corrected by the correlation term U and (ii) the inclusion of SOC may seriously affect the dispersion

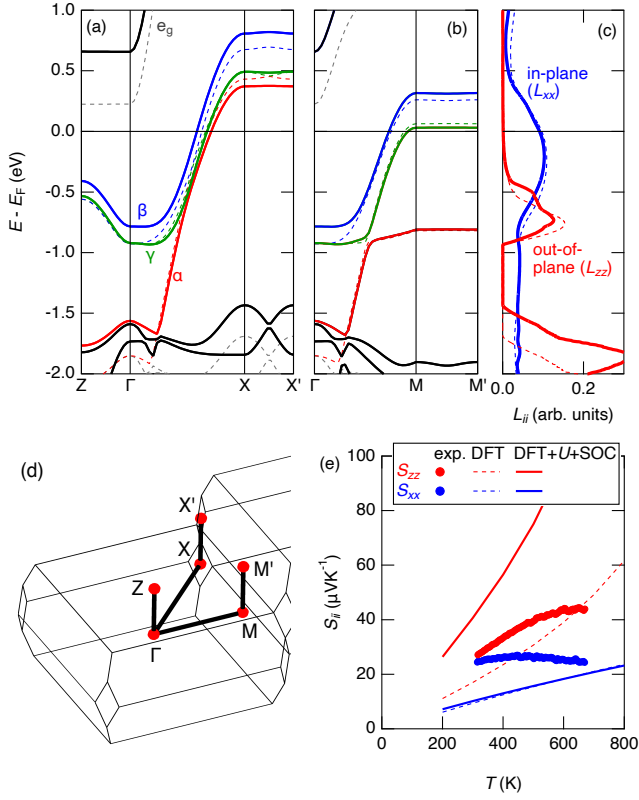


FIG. 4. (a,b) Calculated band structure with DFT+ U +SOC scheme (solid curves) along (a) the Z- Γ -X-X' and (b) the Γ -M-M' lines. The dashed curves represent the results of scalar relativistic calculations and U is not included. The α (red), β (blue), and γ (green) bands cross the Fermi energy E_F indicated by the solid line. (c) The in-plane and out-of-plane transport functions L_{ii} ($ii = xx, zz$). The solid and dashed curves represent the DFT(GGA)+ U +SOC and the DFT calculations, respectively. (d) High-symmetry points and the k path for the band structure in the panels (a) and (b). The points X' and M' locate in the adjacent Brillouin zone. (e) The calculated thermopower S_{ii} for both directions as a function of temperature. The solid symbols are experimental results. The solid and dashed curves represent the DFT+ U +SOC and the DFT calculations, respectively.

along the k_z direction [39], which we focus here. Figures 4(a) and 4(b) show the calculated electronic band structure near the Fermi energy E_F , which well coincides with the results in earlier studies [36–39]. High-symmetry points and the k path are shown in Fig. 4(d). The solid curves represent the DFT+ U +SOC results, while the dashed curves are the conventional GGA results. The β and γ bands at the high-symmetry points Γ and Z split owing to the SOC [39], and the upper e_g bands are shifted upward due to the on-site U . Importantly, the β and γ bands along the Z- Γ -X-X' line are well reproduced with the tight-binding picture shown in Fig. 1(b): the low-energy holes around $E - E_F \approx -0.7$ eV possess the finite velocity along the Z- Γ line. In contrast, the c -axis velocity of the high-energy electrons around $E - E_F \approx +0.5$ eV for the γ band and $\approx +0.8$ eV for the β band becomes almost zero due to the flat dispersion along the X-X' line. No k_z dispersion is also ob-

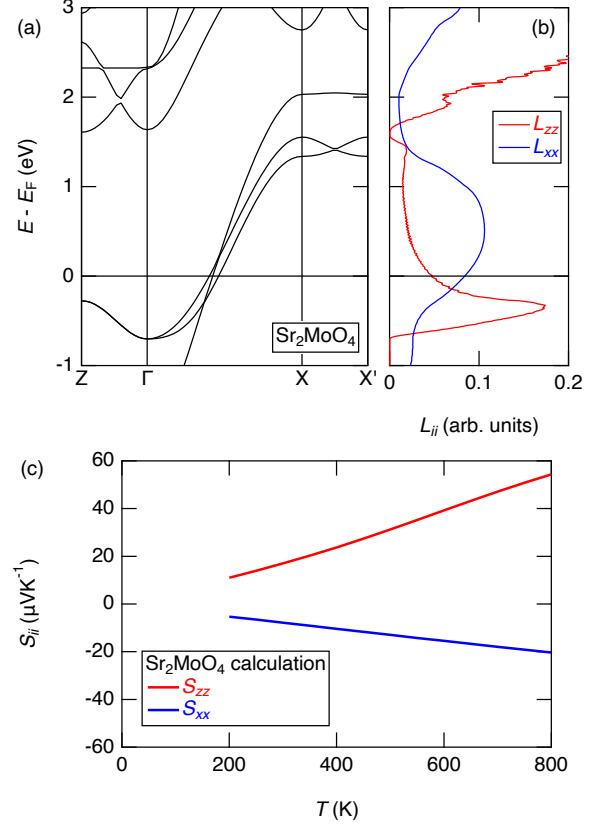


FIG. 5. (a) Calculated band structure of Sr_2MoO_4 with GGA scheme along the Z- Γ -X-X' line. (b) The in-plane and out-of-plane transport functions L_{ii} ($ii = xx, zz$). (c) The calculated thermopower S_{ii} ($ii = xx, zz$) as a function of temperature.

served at the edge of the Brillouin zone along the M-M' line [Fig. 4(b)].

Figure 4(c) shows the in-plane and out-of-plane transport function L_{ii} ($ii = xx, zz$) displayed in the same energy range for Figs. 4(a) and 4(b). Corresponding to the band structure shown in Fig. 4(a), a significant peak structure of L_{zz} is found near $E - E_F \approx -0.7$ eV in contrast to the negligibly small L_{zz} for $E > E_F$. These prominent asymmetry in L_{zz} owing to aforementioned large hole and small electron velocities may lead to the enhanced positive thermopower at high temperatures. Note that although the L_{zz} peak is far from the Fermi energy ($E - E_F \approx -0.7$ eV) compared to the thermal energy $k_B T$ of the present measurement range, this energy difference should become smaller by considering the scattering of correlated carriers accurately [23]. In contrast to highly asymmetric out-of-plane transport function, the in-plane one L_{xx} in Fig. 4(c) seems symmetric around E_F . The thermopower data calculated with the different schemes are shown in Fig. 4(e). Although the experimental data are not reproduced well due to the absence of mass renormalizations from the dynamical real-part of the self-energy [23], which is not included in the present DFT calculation, the enhanced out-of-plane thermopower S_{zz} is obtained owing to the carrier filtering effect.

Interestingly, the out-of-plane thermopower calculated with DFT+ U +SOC results is much larger than that calculated with the DFT data. This difference originates from the upper shift of the β band due to the SOC [39], and the L_{zz} peak near $E - E_F \approx -0.7$ eV is slightly shifted to higher energy in the DFT+ U +SOC results [Fig. 4(c)]. These results thus indicate that the SOC may affect the out-of-plane thermopower significantly. Nevertheless, the calculated thermopower S_{zz} from the DFT+ U +SOC results is much larger than the experimental data of the out-of-plane thermopower. This discrepancy may come from the absence of the self-energy analysis as described before.

We also mention other mechanisms to enhance the high-temperature thermopower. Since this material shows an interesting bad-metallic transport at high temperatures [49], the nature of the incoherent charge transport in such regime is of interest [70]. In particular, the thermopower may be enhanced in the bad-metallic state near the Mott insular phase [71], whereas both in-plane and out-of-plane thermopower may be increased in such a case, which differs from the present results.

To explore the present carrier filtering effect in the bct lattice, we have calculated the electronic structure and the transport function for the related layered oxide Sr_2MoO_4 [72]. The calculation here is performed within the GGA scheme. Figures 5(a) and 5(b) show the band structure, which well reproduce the earlier studies [63, 73], and the transport function L_{ii} for Sr_2MoO_4 , respectively. Similar to the results of Sr_2RuO_4 , large difference in the out-of-plane velocities between the Z- Γ and the X-X' lines is observed for Sr_2MoO_4 , while the small k_z dependence is also observed at around $E - E_F \sim 1.4$ eV. Nevertheless, the out-of-plane transport function L_{zz} is prominently asymmetric around E_F and exhibits a peak at around $E - E_F \sim -0.3$ eV, compared to relatively weak energy dependence of the in-plane transport function L_{xx} . Figure 5(c) shows the calculated thermopower for Sr_2MoO_4 . Indeed, the out-of-plane thermopower S_{zz} shows relatively large, positive values owing to the present hole filter effect. In contrast, the

in-plane thermopower S_{xx} becomes negative because the electron number of the Mo ion is smaller than that in the Ru ion. Thus, Sr_2MoO_4 may also be interesting as a candidate of an oxide goniopolar material with axis-dependent polarity [74]. These results imply that the present carrier filtering may be applicable to wide range of the bct lattice such as K_2NiF_4 -type or related structure [75–78], offering an interesting strategy toward the efficient thermoelectrics.

Note added. In the final stage of completion of this paper, we became aware of the preprint of Daou et al. [79], which reports similar results on the anisotropic thermopower of Sr_2RuO_4 single crystals at high temperatures.

IV. SUMMARY

In summary, we have measured the high-temperature thermopower of Sr_2RuO_4 single crystals for both in-plane and out-of-plane directions. We find that the in-plane thermopower exhibits a weak temperature dependence, which may be understood within the Heikes formula including the three different valence states. Interestingly, the out-of-plane thermopower well exceeds the expected value of the Heikes formula and increases with increasing temperature. Such behavior may originate from the theoretically suggested carrier filtering effect, which may be widely applied to various potential thermoelectrics with the body-centered tetragonal lattice system.

ACKNOWLEDGMENTS

We appreciate R. Nishinakayama, H. Shiina, and R. Taira for the assistance. We thank the machine shop in Department of Mechanical and Aerospace Engineering, Tokyo University of Science, for the use of electrical discharge machine. This work was partly supported by JSPS KAKENHI Grant No. 17H06136 and No. 22H01166.

-
- [1] J. He and T. M. Tritt, Advances in thermoelectric materials research: looking back and moving forward. *Science* **357**, eaak9997 (2017).
 - [2] X.-L. Shi, J. Zou, and Z.-G. Chen, Advanced Thermoelectric Design: From Materials and Structures to Devices. *Chem. Rev.* **120**, 7399-7515 (2020).
 - [3] Q. Yan and M. G. Kanatzidis, High-performance thermoelectrics and challenges for practical devices. *Nat. Mater.* **21**, 503 (2022).
 - [4] K. Behnia, Fundamentals of Thermoelectricity (Oxford University Press, Oxford, UK, 2015).
 - [5] D. Vashaev and A. Shakouri, Improved Thermoelectric Power Factor in Metal-Based Superlattices. *Phys. Rev. Lett.* **92**, 106103 (2004).
 - [6] C. J. Vineis, A. Shakouri, A. Majumdar, and M. G. Kanatzidis, Nanostructured Thermoelectrics: Big Efficiency Gains from Small Features. *Adv. Mater.* **22**, 3970 (2010).
 - [7] I. Terasaki, Y. Sasago, and K. Uchinokura, Large thermoelectric power in NaCo_2O_4 single crystals. *Phys. Rev. B* **56**, R12685(R) (1997).
 - [8] K. Kuroki and R. Arita, “Pudding Mold” Band Drives Large Thermopower in Na_xCoO_2 . *J. Phys. Soc. Jpn.* **76**, 083707 (2007).
 - [9] H. Usui, K. Suzuki, K. Kuroki, S. Nakano, K. Kudo, and M. Nohara, Large Seebeck effect in electron-doped FeAs_2 driven by a quasi-one-dimensional pudding-mold-type band. *Phys. Rev. B* **88**, 075140 (2013).
 - [10] L. D. Hicks and M. S. Dresselhaus, The effect of quantum well structures on the thermoelectric figure of merit. *Phys. Rev. B* **47**, 12727 (1993).
 - [11] H. Ohta, S. Kim, Y. Mune, T. Mizoguchi, K. Nomura, S. Ohta, T. Nomura, Y. Nakanishi, Y. Ikuhara, M. Hirano, H. Hosono, and K. Koumoto, Giant thermoelectric Seebeck coefficient of a two-dimensional electron gas in SrTiO_3 . *Nat. Mater.* **6**, 129 (2007).

- [12] S. Shimizu, M. S. Bahramy, T. Iizuka, S. Ono, K. Miwa, Y. Tokura, and Y. Iwasa, Enhanced thermopower in ZnO two-dimensional electron gas, *Proc. Natl. Acad. Sci. USA* **113**, 6438 (2016).
- [13] N. Kouda, K. Eguchi, R. Okazaki, and M. Tamura, Anomalous scaling law for thermoelectric transport of two-dimensional confined electrons in an organic molecular system. *Phys. Rev. Research* **4**, 043050 (2022).
- [14] A. Maignan, V. Caignaert, B. Raveau, D. Khomskii, and G. Sawatzky, Thermoelectric Power of $\text{HoBaCo}_2\text{O}_{5.5}$: Possible Evidence of the Spin Blockade in Cobaltites. *Phys. Rev. Lett.* **93**, 026401 (2004).
- [15] A. A. Taskin and Y. Ando, Electron-Hole Asymmetry in $\text{GdBaCo}_2\text{O}_{5+x}$: Evidence for Spin Blockade of Electron Transport in a Correlated Electron System. *Phys. Rev. Lett.* **95**, 176603 (2005).
- [16] A. A. Taskin, A. N. Lavrov, and Y. Ando, Transport and magnetic properties of $\text{GdBaCo}_2\text{O}_{5+x}$ single crystals: A cobalt oxide with square-lattice CoO_2 planes over a wide range of electron and hole doping. *Phys. Rev. B* **71**, 134414 (2005).
- [17] A. A. Taskin, A. N. Lavrov, and Y. Ando, Origin of the large thermoelectric power in oxygen-variable $\text{RBaCo}_2\text{O}_{5+x}$ ($R = \text{Gd}, \text{Nd}$). *Phys. Rev. B* **73**, 121101(R) (2006).
- [18] C. F. Chang, Z. Hu, H. Wu, T. Burnus, N. Hollmann, M. Benomar, T. Lorenz, A. Tanaka, H.-J. Lin, H. H. Hsieh, C. T. Chen, and L. H. Tjeng, Spin Blockade, Orbital Occupation, and Charge Ordering in $\text{La}_{1.5}\text{Sr}_{0.5}\text{CoO}_4$. *Phys. Rev. Lett.* **102**, 116401 (2009).
- [19] D. S. Negi, D. Singh, P. A. van Aken, and R. Ahuja, Spin-entropy induced thermopower and spin-blockade effect in CoO . *Phys. Rev. B* **100**, 144108 (2019).
- [20] R. Okazaki and K. Tomiyasu, Prominent electron-hole asymmetry in the thermoelectric transport of LaCoO_3 . *Phys. Rev. B* **105**, 035154 (2022).
- [21] A. Georges and J. Mravlje, Skewed non-Fermi liquids and the Seebeck effect. *Phys. Rev. Research* **3**, 043132 (2021).
- [22] A. Gourgout, G. Grissonnache, F. Laliberté, A. Ataei, L. Chen, S. Verret, J.-S. Zhou, J. Mravlje, A. Georges, N. Doiron-Leyraud, and L. Taillefer, Seebeck Coefficient in a Cuprate Superconductor: Particle-Hole Asymmetry in the Strange Metal Phase and Fermi Surface Transformation in the Pseudogap Phase. *Phys. Rev. X* **12**, 011037 (2022).
- [23] J. Mravlje and A. Georges, Thermopower and Entropy: Lessons from Sr_2RuO_4 . *Phys. Rev. Lett.* **117**, 036401 (2016).
- [24] Y. Maeno, H. Hashimoto, K. Yoshida, S. Nishizaki, T. Fujita, J. G. Bednorz, and F. Lichtenberg, Superconductivity in a layered perovskite without copper. *Nature* **372**, 532 (1994).
- [25] T. M. Rice and M. Sigrist, Sr_2RuO_4 : an electronic analogue of ^3He ? *J. Phys.: Condens. Matter* **7**, L643 (1995).
- [26] A. P. Mackenzie and Y. Maeno, The superconductivity of Sr_2RuO_4 and the physics of spin-triplet pairing. *Rev. Mod. Phys.* **75**, 657 (2003).
- [27] C. Kallin, Chiral p-wave order in Sr_2RuO_4 . *Rep. Prog. Phys.* **75**, 042501 (2012).
- [28] A. P. Mackenzie, T. Scaffidi, C. W. Hicks, and Y. Maeno, Even odder after twenty-three years: The superconducting order parameter puzzle of Sr_2RuO_4 . *npj Quant. Mater.* **2**, 40 (2017).
- [29] S. A. Kivelson, A. C. Yuan, B. Ramshaw, and R. Thomale, A proposal for reconciling diverse experiments on the superconducting state in Sr_2RuO_4 . *npj Quant. Mater.* **5**, 43 (2020).
- [30] A. Pustogow, Y. Luo, A. Chronister, Y.-S. Su, D. A. Sokolov, F. Jerzembeck, A. P. Mackenzie, C. W. Hicks, N. Kikugawa, S. Raghu, E. D. Bauer, and S. E. Brown Constraints on the superconducting order parameter in Sr_2RuO_4 from oxygen-17 nuclear magnetic resonance. *Nature* **574**, 72 (2019).
- [31] K. Ishida, M. Manago, K. Kinjo, and Y. Maeno, Reduction of the ^{17}O Knight Shift in the Superconducting State and the Heat-up Effect by NMR Pulses on Sr_2RuO_4 . *J. Phys. Soc. Jpn.* **89**, 034712 (2020).
- [32] A. Chronister, A. Pustogow, N. Kikugawa, D. A. Sokolov, F. Jerzembeck, C. W. Hicks, A. P. Mackenzie, E. D. Bauer, and S. E. Brown, Evidence for even parity unconventional superconductivity in Sr_2RuO_4 . *Proc. Natl. Acad. Sci. U.S.A.* **118**, e2025313118 (2021).
- [33] S. Benhabib, C. Lupien, I. Paul, L. Berges, M. Dion, M. Nardone, A. Zitouni, Z. Q. Mao, Y. Maeno, A. Georges, L. Taillefer, and C. Proust Ultrasound evidence for a two-component superconducting order parameter in Sr_2RuO_4 . *Nat. Phys.* **17**, 194 (2021).
- [34] S. Ghosh, A. Shekhter, F. Jerzembeck, N. Kikugawa, D. A. Sokolov, M. Brando, A. P. Mackenzie, C. W. Hicks, and B. J. Ramshaw, Thermodynamic evidence for a two-component superconducting order parameter in Sr_2RuO_4 . *Nat. Phys.* **17**, 199 (2021).
- [35] V. Grinenko, S. Ghosh, R. Sarkar, J.-C. Orain, A. Nikitin, M. Elender, D. Das, Z. Guguchia, F. Brückner, M. E. Barber, J. Park, N. Kikugawa, D. A. Sokolov, J. S. Bobowski, T. Miyoshi, Y. Maeno, A. P. Mackenzie, H. Luetkens, C. W. Hicks, and H.-H. Klauss, Split superconducting and time-reversal symmetry-breaking transitions in Sr_2RuO_4 under stress. *Nat. Phys.* **17**, 748 (2021).
- [36] T. Oguchi, Electronic band structure of the superconductor Sr_2RuO_4 . *Phys. Rev. B* **51**, 1385 (1995).
- [37] D. J. Singh, Relationship of Sr_2RuO_4 to the superconducting layered cuprates. *Phys. Rev. B* **52**, 1358 (1995).
- [38] I. Hase and Y. Nishihara, Electronic Structures of Sr_2RuO_4 and Sr_2RhO_4 . *J. Phys. Soc. Jpn.* **65**, 3957 (1996).
- [39] M.W. Haverkort, I. S. Elfimov, L. H. Tjeng, G. A. Sawatzky, and A. Damascelli, Strong Spin-Orbit Coupling Effects on the Fermi Surface of Sr_2RuO_4 and Sr_2RhO_4 . *Phys. Rev. Lett.* **101**, 026406 (2008).
- [40] O. Gingras, R. Nourafkan, A.-M. S. Tremblay, and M. Côté, Superconducting Symmetries of Sr_2RuO_4 from First-Principles Electronic Structure. *Phys. Rev. Lett.* **123**, 217005 (2019).
- [41] A. P. Mackenzie, S. R. Julian, A. J. Diver, G. J. McMullan, M. P. Ray, G. G. Lonzarich, Y. Maeno, S. Nishizaki, and T. Fujita, Quantum Oscillations in the Layered Perovskite Superconductor Sr_2RuO_4 . *Phys. Rev. Lett.* **76**, 3786 (1996).
- [42] T. Yokoya, A. Chainani, T. Takahashi, H. Ding, J. C. Campuzano, H. Katayama-Yoshida, M. Kasai, and Y. Tokura, Angle-resolved photoemission study of Sr_2RuO_4 . *Phys. Rev. B* **54**, 13311 (1996).
- [43] A. Damascelli, D. H. Lu, K. M. Shen, N. P. Armitage, F. Ronning, D. L. Feng, C. Kim, Z.-X. Shen, T. Kimura, Y. Tokura, Z. Q. Mao, and Y. Maeno, Fermi Surface, Surface States, and Surface Reconstruction in Sr_2RuO_4 . *Phys. Rev. Lett.* **85**, 5194 (2000).
- [44] K. M. Shen, N. Kikugawa, C. Bergemann, L. Balicas, F. Baumberger, W. Meevasana, N. J. C. Ingle, Y. Maeno, Z.-X. Shen, and A. P. Mackenzie, Evolution of the Fermi Surface and Quasiparticle Renormalization through a van Hove Singularity in $\text{Sr}_{2-y}\text{La}_y\text{RuO}_4$. *Phys. Rev. Lett.* **99**, 187001 (2007).
- [45] A. Tamai, M. Zingl, E. Rozbicki, E. Cappelli, S. Riccò, A. de la Torre, S. McKeown Walker, F. Y. Bruno, P. D. C. King, W. Meevasana, M. Shi, M. Radović, N. C. Plumb, A. S. Gibbs, A. P. Mackenzie, C. Berthod, H. U. R. Strand, M. Kim, A. Georges, and F. Baumberger, *Phys. Rev. X* **9**, 021048 (2019).

- [46] H. Yoshino, K. Murata, N. Shirakawa, Y. Nishihara, Y. Maeno, and T. Fujita, Thermopower of a Layered Perovskite Superconductor, Sr_2RuO_4 . *J. Phys. Soc. Jpn.* **65**, 1548 (1996).
- [47] X. F. Xu, Z. A. Xu, T. J. Liu, D. Fobes, Z. Q. Mao, J. L. Luo, and Y. Liu, Band-Dependent Normal-State Coherence in Sr_2RuO_4 : Evidence from Nernst Effect and Thermopower Measurements. *Phys. Rev. Lett.* **101**, 057002 (2008).
- [48] T. Yamanaka, R. Okazaki, and H. Yaguchi, Enhanced Seebeck coefficient through magnetic fluctuations in $\text{Sr}_2\text{Ru}_{1-x}\text{M}_x\text{O}_4$ ($M = \text{Co}, \text{Mn}$). *Phys. Rev. B* **105**, 184507 (2022).
- [49] A. W. Tyler, A. P. Mackenzie, S. NishiZaki, and Y. Maeno, High-temperature resistivity of Sr_2RuO_4 : Bad metallic transport in a good metal. *Phys. Rev. B* **58**, R10107 (1998).
- [50] Z. Q. Mao, Y. Maeno, and H. Fukazawa, Crystal growth of Sr_2RuO_4 , *Mater. Res. Bull.* **35**, 1813 (2000).
- [51] K. Yamamoto, T. Yamazaki, T. Yamanaka, D. Ueta, H. Yoshizawa, and H. Yaguchi, Anisotropic Pressure Effects on Superconductivity in $\text{Fe}_{1+y}\text{Te}_{1-x}\text{S}_x$. *J. Phys. Soc. Jpn.* **87**, 054705 (2018).
- [52] Y. Ikeda, K. Saito, and R. Okazaki, Thermoelectric transport in the layered $\text{Ca}_3\text{Co}_{4-x}\text{Rh}_x\text{O}_9$ single crystals. *J. Appl. Phys.* **119**, 225105 (2016).
- [53] H. Sakabayashi and R. Okazaki, Crossover from itinerant to localized states in the thermoelectric oxide $[\text{Ca}_2\text{CoO}_3]_{0.62}[\text{CoO}_2]$. *Phys. Rev. B* **103**, 125119 (2021).
- [54] K. Kurita, M. Yagisawa, and R. Okazaki, Electrical resistivity and thermopower of hole-doped delafossite CuCoO_2 polycrystals. *Jpn. J. Appl. Phys.* **60**, 013001 (2021).
- [55] P. Giannozzi *et al.*, QUANTUM ESPRESSO: a modular and open-source software project for quantum simulations of materials. *J. Phys.: Condens. Matter* **21**, 395502 (2009).
- [56] P. Giannozzi *et al.*, Advanced capabilities for materials modelling with Quantum ESPRESSO. *J. Phys.: Condens. Matter* **29**, 465901 (2017).
- [57] P. Giannozzi *et al.*, Quantum ESPRESSO toward the exascale. *J. Chem. Phys.* **152**, 154105 (2020).
- [58] H.-L. Huang and H.-t. Jeng, Orbital ordering and magnetism in layered perovskite Ruthenate Sr_2RuO_4 . *Sci. Rep.* **10**, 7089 (2020).
- [59] P. Giannozzi, D. Volja, D. Kozinsky, M. Fornari, N. Marzari, G. K. H. Madsen, J. Carrete, and M. J. Verstraete, BoltzWann: A code for the evaluation of thermoelectric and electronic transport properties with a maximally-localized Wannier functions basis. *Comp. Phys. Commun.* **185**, 422-429 (2014).
- [60] G. K.H. Madsen, BoltzTraP. A code for calculating band-structure dependent quantities. *Comput. Phys. Commun.* **175**, 67 (2006).
- [61] N. Keawprak, R. Tu, and T. Goto, Thermoelectric Properties of Sr-Ru-O Compounds Prepared by Spark Plasma Sintering. *Mater. Trans.* **49**, 600 (2008).
- [62] A. Georges, L. de' Medici, and J. Mravlje, Strong Correlations from Hund's Coupling. *Annu. Rev. Condens. Matter Phys.* **4**, 137 (2013).
- [63] Jonathan Karp, Max Bramberger, Martin Grundner, Ulrich Schollwöck, Andrew J. Millis, and Manuel Zingl, Sr_2MoO_4 and Sr_2RuO_4 : Disentangling the Roles of Hund's and van Hove Physics. *Phys. Rev. Lett.* **125**, 166401 (2020).
- [64] W. Kobayashi, I. Terasaki, M. Mikami, and R. Funahashi, Negative Thermoelectric Power Induced by Positive Carriers in $\text{CaMn}_{3-x}\text{Cu}_x\text{Mn}_4\text{O}_{12}$. *J. Phys. Soc. Jpn.* **73**, 523 (2004).
- [65] Y. Klein, S. Hébert, A. Maignan, S. Kolesnik, T. Maxwell, and B. Dabrowski, Insensitivity of the band structure of substituted SrRuO_3 as probed by Seebeck coefficient measurements. *Phys. Rev. B* **73**, 052412 (2006).
- [66] S. Hébert, R. Daou, and A. Maignan, Thermopower in the quadruple perovskite ruthenates. *Phys. Rev. B* **91**, 045106 (2015).
- [67] P. M. Chaikin and G. Beni, Thermopower in the correlated hopping regime. *Phys. Rev. B* **13**, 647 (1976).
- [68] J.-P. Doumerc, Thermoelectric Power for Carriers in Localized States: A Generalization of Heikes and Chaikin-Beni Formulae. *J. Solid State Chem.* **109**, 419 (1994).
- [69] W. Koshibae, K. Tsutsui, and S. Maekawa, Thermopower in cobalt oxide. *Phys. Rev. B* **62**, 6869 (2000).
- [70] Sean A. Hartnoll, Theory of universal incoherent metallic transport. *Nat. Phys.* **11**, 54 (2014).
- [71] V. Zlatić, G. R. Boyd, and J. K. Freericks, Universal thermopower of bad metals. *Phys. Rev. B* **89**, 155101 (2014).
- [72] S.-i. Ikeda, N. Shirakawa, H. Bando, and Y. Ootuka, Orbital-Degenerate Paramagnetic Metal Sr_2MoO_4 : An Electronic Analogue to Sr_2RuO_4 . *J. Phys. Soc. Jpn.* **69**, 3162 (2000).
- [73] I. Hase, S.-i. Ikeda, N. Shirakawa, and J. K. Stalick, Electronic Structure of Sr_2MoO_4 . *J. Low Temp. Phys.* **131**, 269 (2003).
- [74] K. Uchida and J P. Heremans, Thermoelectrics: from Longitudinal to Transverse. *Joule* **6**, 2240 (2022).
- [75] P. Ganguly and C.N.R. Rao, Electron transport properties of transition metal oxide systems with the K_2NiF_4 structure. *Mater. Res. Bull.* **8**, 405 (1973).
- [76] J. Matsuno, Y. Okimoto, Z. Fang, X. Z. Yu, Y. Matsui, N. Nagaosa, M. Kawasaki, and Y. Tokura, Metallic Ferromagnet with Square-Lattice CoO_2 Sheets. *Phys. Rev. Lett.* **93**, 167202 (2004).
- [77] P. K. Pandey, R. J. Choudhary, and D. M. Phase, Magnetic behavior of layered perovskite Sr_2CoO_4 thin film. *Appl. Phys. Lett.* **103**, 132413 (2013).
- [78] R. S. Perry, F. Baumberger, L. Balicas, N. Kikugawa, N. J. C. Ingle, A. Rost, J. F. Mercure, Y. Maeno, Z. X. Shen, and A. P. Mackenzie, Sr_2RhO_4 : a new, clean correlated electron metal. *New J. Phys.* **8**, 175 (2006).
- [79] R. Daou, S. Hébert, Gaël Grissonnanche, E. Hassinger, L. Taillefer, H. Taniguchi, Y. Maeno, A. S. Gibbs, and A. P. Mackenzie, Anisotropic Seebeck coefficient of Sr_2RuO_4 in the incoherent regime. *Phys. Rev. B* **108**, L121106 (2023).